ARTICLE

Raman Spectrum of Er-Y-codoped ZrO_2 and Fluorescence Properties of Er^{3+}

Jun He, Meng-fei Luo*, Ling-yun Jin, Mai He, Ping Fang, Yun-long Xie

Key Laboratory for Reactive Chemistry on Solid Surfaces of Zhejiang, Institute of Physical Chemistry, Zhejiang Normal University, Jinhua 321004, China

(Dated: Received on March 28, 2006; Accepted on July 16, 2006)

Er-Y-codoped ZrO_2 mixed oxides with monoclinic, tetragonal and cubic structures were prepared by a sol-gel method. The crystal structure of ZrO_2 matrix and the effect of the ZrO_2 phases on the fluorescence properties of Er^{3+} were studied using Raman spectroscopy. The results indicated that the fluorescence properties of Er^{3+} depend on its local ZrO_2 crystal structures. As ZrO_2 matrix transferred from monoclinic to tetragonal and cubic phase, the Raman and fluorescence bands of Er^{3+} decreased in intensities and tended to form a single peak. With 632.8 nm excitation, the bands between 640 and 680 nm were attributed to the fluorescence of Er^{3+} in the ZrO_2 environment. However, only the fluorescence was observed and no Raman spectra were seen under 514.5 nm excitation, while only Raman spectra were observed under 325 nm excitation. UV Raman spectroscopy was found to be more sensitive in the surface region while the information provided by XRD mainly came from the bulk. The phase with lower symmetry forms more easily on the surface than in the bulk.

Key words: ZrO_2, Er^{3+}, Raman spectrum, XRD, Fluorescence properties

I. INTRODUCTION

Rare-earth (RE) ions with abundant electronic bands providing the conditions for multi-bands transition are ideal excited ions for optical materials [1-4]. RE ions doped ZrO_2 is frequently used in optical materials for its low phonon energy. There is a nonradiative relaxation from matrix to excited ions in the monoclinic ZrO_2, which favors the fluorescence emission of ZrO_2 doped by Eu^{3+}, Sm^{3+}, Er^{3+} and other RE ions [5-8]. However, the fluorescence bands depend on local ZrO_2 structures. For example, Er^{3+} shows different fluorescence properties in ZrO_2 host with three different phases [9]. The studies indicate that doping metal oxides such as CaO, MgO, Y_2O_3 and Yb_2O_3 can promote ZrO_2 transfer from monoclinic to tetragonal and cubic [10-13]. The surface properties of the particle are very important for catalytic reactions and luminescence emissions [14,15]. Structures on the surface and the bulk of ZrO_2 are usually different [16,17], so it is necessary to distinguish the surface and bulk structures of materials and their effects on the fluorescence properties. Li *et al.* studied ZrO_2 and Y_2O_3 doped ZrO_2 and suggested that UV Raman spectroscopy is more sensitive to the surface region of zirconia because it shows a strong absorption in the UV region, so the different information from the surface and the bulk can be distinguished [16,17]. In this work, the surface and bulk structures of Er-Y-codoped ZrO_2 were studied using Raman spectroscopy with different excitation wavelengths and XRD. Er^{3+} fluorescence properties in different ZrO_2 phases were also studied.

*Author to whom correspondence should be addressed. E-mail: mengfeiluo@zjnu.cn

II. EXPERIMENTS

A. Preparation of Er-Y-ZrO_2

The Er-Y-ZrO_2 samples were prepared by a sol-gel method. The detailed process is as follows: $Zr(NO_3)_4$, $Y(NO_3)_3$ and $Er(NO_3)_3$ aqueous solutions were mixed together in a proper ratio, then citric acid was added at 90 °C under stirring until the gel was obtained. The gel was dried at 110 °C for 24 h. Finally it was calcined at 950 °C for 4 h. The samples are denoted as Er-ZrO_2, Er-Y_5-ZrO_2, Er-Y_{15}-ZrO_2 and Er-Y_{25}-ZrO_2. The Y content (mol ratio) is 0%, 5%, 15% and 25% of ZrO_2, respectively, and Er^{3+} content is 0.1 mol% of the sum of Y^{3+} and Zr^{4+}.

B. Characterizations of Er-Y-ZrO_2

Visible Raman spectra were obtained with a Renishaw RM1000 confocal microscope with excitation wavelengths of 632.8 and 514.5 nm. Ultraviolet visible (UV) Raman spectra were obtained on a Jobin Yvon LabRamHRUV with an excitation wavelength of 325 nm.

X-ray diffraction (XRD) patterns were collected on a PHILIPS PW3040/60 powder diffractometer operating at 40 kV/40 mA using Cu Kα radiation in the 2θ range from 20° to 80° with a scan rate of 4°/min. Phase composition and cell parameters were calculated by Rietveld analysis method.

TABLE I Phase composition, cell parameter and mean crystalline size of Er-Y-ZrO_2 samples

Sample	Phase	Cell parameter/nm			Mean crystalline/nm
		a	*b*	*c*	
Er-ZrO_2	*m*-ZrO_2+*t*-ZrO_2	0.5146	0.5185	0.5314	33.3
Er-Y_5-ZrO_2	*t*-ZrO_2	0.3606	–	0.5182	50.0
Er-Y_{15}-ZrO_2	*c*-ZrO_2	0.5118	–	–	40.2
Er-Y_{25}-ZrO_2	*c*-ZrO_2	0.5148	–	–	52.6

Transmission electron microscopy (TEM) investigations were carried out using a JEM-1200 EX microscope operating at 80 kV.

UV-Visible diffuse reflectance spectra were recorded on a Thermo Evolution 500 spectrophotometer equipped with a labsphere RSA-UC-40.

III. RESULTS AND DISCUSSION

Figure 1 shows the XRD patterns of the Er-Y-ZrO_2 samples. For the Er-ZrO_2 sample, peaks attributed to *m*-ZrO_2 and *t*-ZrO_2 were observed. The proportion of the *m*-ZrO_2 was higher than that of *t*-ZrO_2. However, a single tetragonal phase was observed for the Er-Y_5-ZrO_2 sample, while for both Er-Y_{15}-ZrO_2 and Er-Y_{25}-ZrO_2 samples only cubic phase was observed [18]. The phase composition, cell parameter and mean crystalline size of Er-Y-ZrO_2 samples are listed in Table I. The cell volume of cubic phase increased from 0.5118 nm to 0.5148 nm with the increase of Y content from 15% to 25%. This is because the ionic radius of Y^{3+} (0.110 nm) is larger than that of Zr^{4+} (0.084 nm), and the cell volume increases when Y^{3+} replaces Zr^{4+} forming the solid solution. Moreover, this indicated the formation of the Er-Y-ZrO_2 solid solutions.

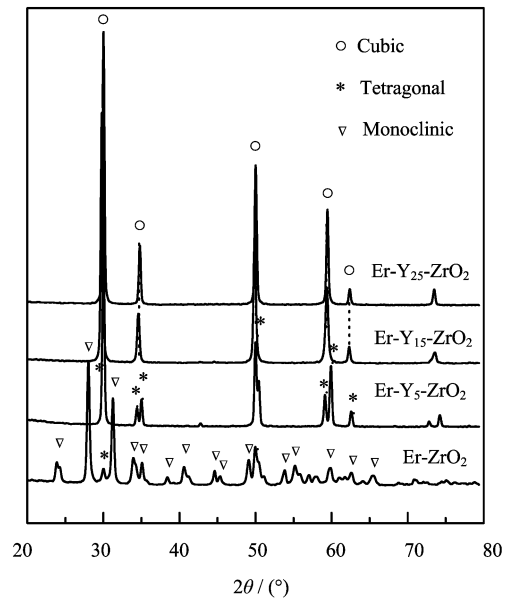

FIG. 1 XRD patterns of Er-Y-ZrO_2 samples.

Figure 2 shows the TEM images of samples Er-Y_5-ZrO_2. It shows that the size distribution of the particles is uniform. The particle sizes estimated from the TEM images are about 50 nm, which is consistent with that calculated by the Scherrer equation.

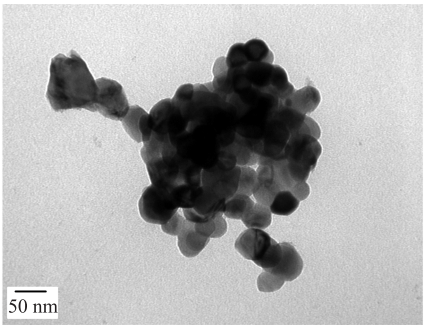

FIG. 2 TEM images of Er-Y_5-ZrO_2 sample.

Figure 3 shows the UV-Vis diffuse reflectance spec-

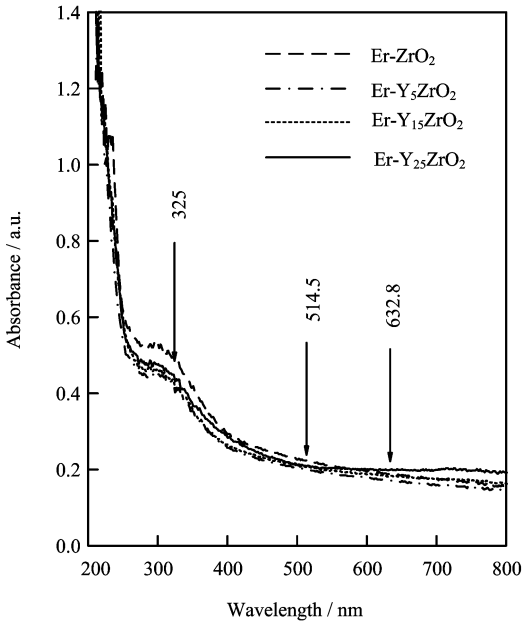

FIG. 3 UV-Visible diffuse reflectance spectra of Er-Y-ZrO_2 samples.

ISSN 1003-7713/DOI:10.1360/cjcp2007.20(1).90.5

tra of Er-Y-ZrO_2 samples with different phases. It can be seen that all the samples show an absorption band between 300 and 400 nm, and the absorption intensity decreases with increasing wavelength. The samples show hardly any absorption at 632.8 nm but a little at 514.5 nm. Therefore, when a sample is excited, the information from the bulk decreases since the sample strongly absorbs the 325 nm excitation laser light and the scattering light, so the Raman spectra obtains more information from the surface top region of a sample than from the bulk.

Figure 4 shows the Raman and fluorescence spectra of the Er-Y-ZrO_2 samples under 632.8 nm excitation where the coordinate "cm^{-1}" corresponds to Raman spectra while "nm" to fluorescence spectra. As shown in the Raman spectra, the major bands appear at 175, 187, 331, 345, 380, 474, 492, 613, 632 and 735 cm^{-1}, and the weak bands at 223, 306, 525 and 560 cm^{-1} for the Er-ZrO_2 sample. These Raman bands are assigned to the Raman-active modes for the m-ZrO_2. In addition, there are two weak bands at 264 and 643 cm^{-1} for the t-ZrO_2. Obviously, the Er-ZrO_2 sample is mainly composed of m-ZrO_2 together with a minorproportion of t-ZrO_2 [11,19], which agree with the XRD results. Strong fluorescence bands between 640 and 680 nm were observed corresponding to the $^4F_{9/2}\rightarrow{}^4I_{15/2}$ [20,21] transition of Er^{3+}. By coincidence, the Raman bands of ZrO_2 are mostly under 800 cm^{-1} (about 667 nm), so there are some overlaps of fluorescence and Raman bands under 800 cm^{-1}. For the Er-Y_5-ZrO_2 sample, the spectra become simpler, and strong bands at 264, 320 and 553 cm^{-1} together with weak bands at 143 and 463 cm^{-1} were observed. This indicates that the Er-Y_5-ZrO_2 has tetragonal structure, which agrees with the XRD results. As the ZrO_2 matrix transfers from monoclinic to tetragonal phase, the fluorescence bands of Er^{3+} between 640 and 680 nm become a single band at about 680 nm. When the Y content increases to 15% and 25%, none of the Raman bands assigned to the m-ZrO_2 or t-ZrO_2 were observed except two at about 492 and 550 cm^{-1}. They may be due to the overlap of Raman bands and fluorescence bands of the t-ZrO_2. From Fig.4, it can be seen that the symmetry of the fluorescence bands of Er^{3+} in the host with cubic phase is much better than that in Er-Y_5-ZrO_2 with tetragonal phase.

In order to clarify the fluorescence properties of Er^{3+} in the different crystal structure environments, Figure 5 shows the Raman and fluorescence spectra of Er-Y-ZrO_2 samples with 514.5 nm excitation. According to Ref.[22], the emission bands observed at about 525 and 550 nm are observed, assigned to $^2H_{11/2}\rightarrow{}^4I_{15/2}$ [9] and $^4S_{3/2}\rightarrow{}^4I_{15/2}$ [23] transitions, respectively. Red emission was observed from the $^4F_{9/2}\rightarrow{}^4I_{15/2}$ [24] transition at about 650 nm. The intensities of green emission at 550 nm from the $^4S_{3/2}\rightarrow{}^4I_{15/2}$ transition is stronger than that of the other two emissions. Consequently, it is considered that the Raman information of the Er-Y-codoped ZrO_2 samples can not be observed with 514.5 nm excitation. With the sample doped by Y^{3+}, much less splitting of emission bands was observed in Er-Y_5-ZrO_2, compared to Er-ZrO_2. It is believed that the two

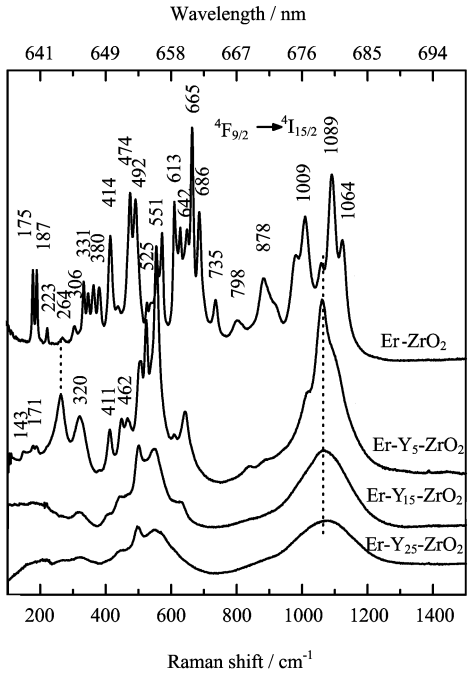

FIG. 4 Raman and fluorescence spectra of Er-Y-ZrO_2 samples at 632.8 nm excitation.

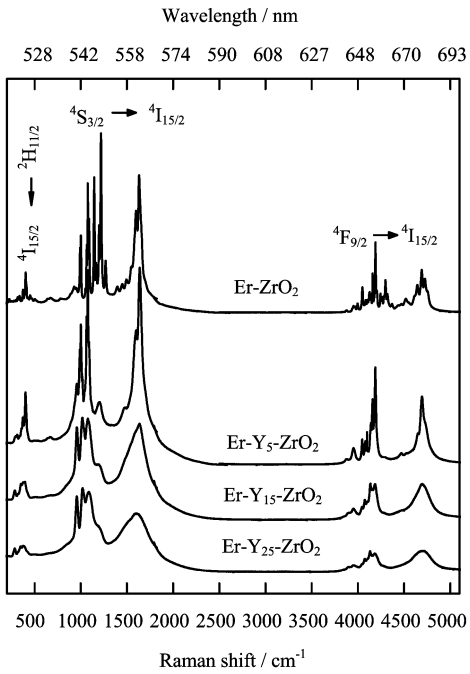

FIG. 5 Raman and fluorescence spectra of Er-Y-ZrO_2 samples at 514.5 nm excitation.

ISSN 1003-7713/DOI:10.1360/cjcp2007.20(1).90.5

reasons for this are as follows: one is that the presence of Y^{3+} makes the ZrO_2 matrix transfer from monoclinic to tetragonal phase; the other is that Y^{3+} is presumed to prevent the cluster formation of Er^{3+} [22]. Similarly, it makes the fluorescence emission of Er^{3+} become more prominent in the Er-Y_{15}-ZrO_2 and Er-Y_{25}-ZrO_2 samples with cubic phase. That is to say, the symmetry of Er^{3+} becomes better when the host crystal phase transfers from monoclinic to tetragonal and cubic. As shown in Fig.5, the shape and position of the emission peaks in Er-Y_{15}-ZrO_2 and Er-Y_{25}-ZrO_2 are similar, which indicates there is very little difference between the two phases [9]. Therefore, it can be concluded that the ZrO_2 species with different crystal phases can be distinguished by the fluorescence spectra of Er-Y-ZrO_2 samples following 514.5 nm excitation. Moreover, a group of fluorescence emission bands at about 650 nm for the Er-Y-ZrO_2 samples are observed. It can be further proved from Fig.5 that for the Er-Y_5-ZrO_2 sample following 632.8 nm excitation, the Raman bands at about 650 nm contain some fluorescence emissions of Er^{3+}. It also suggests that the Er-Y_{15}-ZrO_2 and Er-Y_{25}-ZrO_2 samples are stable in the cubic structure.

Figure 6 shows the UV Raman spectra of Er-Y-ZrO_2 samples. For UV Raman spectroscopy, only Raman scattering can be obtained since the fluorescence is avoided. For the Er-ZrO_2 sample, Raman bands at 331, 378, and 474 cm^{-1} together with weak bands at 303, 345, 499, 535, 632, and 752 cm^{-1} are observed, which are attributed to the m-ZrO_2. For both Er-Y_5-ZrO_2 and Er-Y_{15}-ZrO_2 samples, Raman bands at 266, 321, 461, 612 and 640 cm^{-1} were observed, which indicates only tetragonal phase was formed. For the Er-Y_{25}-ZrO_2 sample, there was not only a strong Raman band at 600 cm^{-1} assigned to c-ZrO_2, but also a band at 330 cm^{-1}. It is believed that the band at 330 cm^{-1} is attributable to a metastable tetragonal phase (t' phase) in the Er-Y_{25}-ZrO_2 sample [25]. However, according to the XRD characterization, only cubic phase is formed in both the Er-Y_{15}-ZrO_2 and Er-Y_{25}-ZrO_2 samples.

To summarize Raman experiments with different excitation and UV-Vis diffuse reflectance, it was found that the information from the bulk of a sample could be detected by Raman spectroscopy with 632.8 nm excitation while that from the surface region could be detected selectively by UV Raman spectroscopy [16,17]. Accordingly, the differences in phases between the characterizations of UV Raman and XRD result from the different phase structures in the surface region and the bulk. This indicates that the structure of the surface of the sample is tetragonal phase while the inner structure is cubic, and the surface easily produces phases with low symmetry. Seen from Fig.3, the samples show a little absorption at 514.5 nm. Consequently, it is concluded that the obtained information is closer to the bulk under 514.5 nm excitation. Therefore, when excited under 514.5 nm, the fluorescence peaks (Fig.5) should be assigned to the fluorescence emissions of doped Er^{3+} in the cubic host.

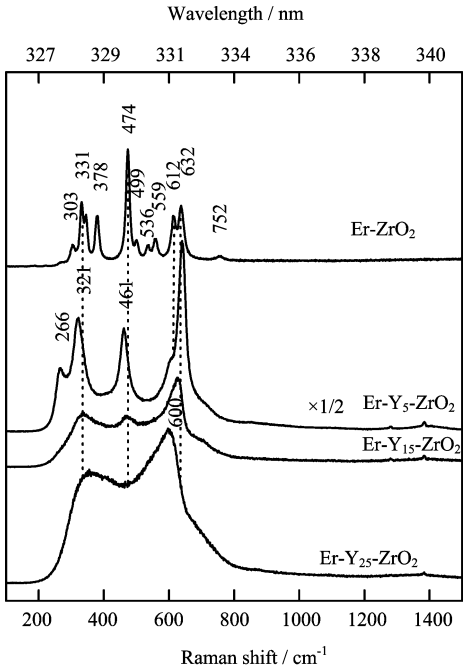

FIG. 6 UV Raman spectra of Er-Y-ZrO_2 samples.

IV. CONCLUSION

The crystal structure of ZrO_2 matrix and the effect of the ZrO_2 phases on the fluorescence properties of Er^{3+} were studied using Raman spectroscopy, UV-Vis diffuse reflectance and XRD. It was found that the fluorescence properties of doped Er^{3+} depend on the local structure around it. As the ZrO_2 matrix transfers from monoclinic to tetragonal and cubic phase, the symmetry of Er^{3+} spectra shapes increases, and the number of the Raman and fluorescence bands decreases in a trend toward a single peak. Therefore, it is concluded that the ZrO_2 species with different crystal phases can be distinguished by the fluorescence spectra of Er-Y-ZrO_2 samples following 514.5 nm excitation. The surface and bulk structures of ZrO_2 and their effects on the fluorescence properties were also studied. UV Raman spectroscopy was found to be more sensitive in the surface region while the information supplied by XRD mainly comes from the bulk, and the lower symmetry phase forms more easily on the surface than that in the bulk.

V. ACKNOWLEDGMENT

This work was supported by the National Natural Science Foundation of China (No.20473075).

ISSN 1003-7713/DOI:10.1360/cjcp2007.20(1).90.5

[1] H. Q. Liu, C. F. Wu, G. S. Qin, W. P. Qin, D. Zhao, J. S. Zhang, S. Z. Lv and X. G. Ren, Chin. J. Lumin. **24**, 181 (2003).
[2] H. Guo, N. Dong, M. Yin, W. P. Zhang, L. R. Lou and S. D. Xia, J. Phys. Chem. **108**, 19206 (2004).
[3] X. G. Wang, H. Y. Wu, D. T. Xie, S. P. Weng and J. G. Wu, Chin. J. Chem. Phys. **14**, 330 (2001).
[4] M. J. Huang, G. D. Xu, X. T. Zhang and Y. J. Mo, Chin. J. Chem. Phys. **13**, 321 (2000).
[5] E. Deíla Rosa-Cruz, L. A. Díaz-Torres, P. Salas, V. M. Castaño and J. M. Hernández, J. Phys. D: Appl. Phys. **34**, 83 (2001).
[6] H. Q. Liu, L. L. Wang and W. P. Qin, Chin. Phys. Soc. **53**, 282 (2004).
[7] C. Urlacher, C. M. de Lucas, E. Bernstein, B. Jacquier and J. Mugnier, J. Opt. Mater. **12**, 20 (1999).
[8] X. Wang, X. G. Kong, G. Y. Shan, Y. Yu, Y. J. Sun, L. Y. Feng, K. F. Chao, S. Z. Lu and Y. J. Li, J. Phys. Chem. B **108**, 18408 (2004).
[9] N. Maeda, N. Wade, H. Onoda, A. Maegawa and K. Kojima, Thin Solid Films. **445**, 384 (2003).
[10] M. Yashima, K. Ohtake, M. Kakihana, H. Arashi and M. Yoshimura, J. Phys. Chem. Solids. **57**, 17 (1996).
[11] F. H. Liao, L. Zhang, J. R. Li, G. Xu, G. B. Li, S. H. Zhang and S. Gao, J. Solid. State. Chem. **176**, 275 (2003).
[12] T. Czeppe, P. Zieba, W. Baliga, E. Dobrev and A. Pawlowski, Mater. Chem. Phys. **81**, 313 (2003).
[13] K. A. Khor and J. Yang, Matter. Lett. **31**, 26 (1997).
[14] M. Morita, N. Miyazaki, S. Murakami, M. Herren and D. Rau, J. Lumin. **76**&**77**, 238 (1998).
[15] R. Xu, X. Wang, D. S. Wang, K. B. Zhou and Y. D. Li, J. Catal. **237**, 426 (2006).
[16] C. Li and M. J. Li, J. Raman. Spectrosc. **33**, 301 (2002).
[17] M. J. Li, Z. C. Feng, G. Xiong, P. L. Ying, Q. Xin and C. Li, J. Phys. Chem. B **105**, 8107 (2001).
[18] F. S. De Vicente, A. C. De Castro, M. F. De Souza and M. Siu Li, Thin. Solid Films **418**, 223 (2002).
[19] J. Q. Gu, W. Yue and Y. Y. Cai, Chin. J. light Scattering. **6**, 77 (1994).
[20] P. Salas, C. Angeles-Chávez, J. A. Montoya, E. Dea Rosa, L. A. Diaz-Torres, H. Desirena, A. Martínez, M. A. Romero-Romo and J. Morales, J. Opt. Mater. **27**, 1298 (2005).
[21] J. A. Capobianco, F. Vetrone and J. C. Boyer, J. Phys. Chem. B **106**, 1182 (2002).
[22] A. Patra, C. S. Friend, R. Kapoor and P. N. Prasad, J. Phys. Chem. B **106**, 1910 (2002).
[23] F. Vetrone, J. C. Boyer, J. A. Capobianco, A. Speghini and M. Bettinelli, Chem. Mater. **15**, 2737 (2003).
[24] F. Vetrone, J. C. Boyer and J. A. Capobianco, J. Phys. Chem. B **106**, 5623 (2002).
[25] A. A. Sobol and Yu. K. Voronko, J. Phys. Chem. Solids **65**, 1106 (2004).

ISSN 1003-7713/DOI:10.1360/cjcp2007.20(1).90.5